the FEBS Journal

MINIREVIEW

Weak protein–ligand interactions studied by small-angle X-ray scattering

Anne T. Tuukkanen and Dmitri I. Svergun

EMBL Hamburg c/o DESY, Hamburg, Germany

Keywords
ab initio modeling; polydispersity; rigid body modeling; small-angle X-ray scattering; transient protein-ligand interactions

Correspondence
D. I. Svergun, EMBL Hamburg c/o DESY, Building 25A, Notkestraße 85, 22603 Hamburg, Germany
Fax: +49 40 89 902 149
Tel: +49 40 89 902 110
E-mail: svergun@embl-hamburg.de

(Received 1 October 2013, revised 22 January 2014, accepted 28 February 2014)

doi:10.1111/febs.12772

Small-angle X-ray scattering (SAXS) is a powerful technique for studying weak interactions between proteins and their ligands (other proteins, DNA/RNA or small molecules) in solution. SAXS provides knowledge about the equilibrium state, the stoichiometry of binding and association–dissociation processes. The measurements are conducted in a solution environment that allows easy monitoring of modifications in protein–ligand association state upon environmental changes. Model-free parameters such as the molecular mass of a system and the radius of gyration can be obtained directly from the SAXS data and give indications about the association state. SAXS is also widely employed to build models of biological assemblies at a resolution of approximately 10–20 Å. Low-resolution shapes can be generated *ab initio*, although more detailed and biologically interpretable information can be obtained by hybrid modelling. In the latter approach, composite structures of protein–ligand complexes are constructed using atomic models of individual molecules. These may be predicted homology models or experimental structures from X-ray crystallography or NMR. This review focuses on using SAXS data to model structures of protein–ligand complexes and to study their dynamics. The combination of SAXS with other methods such as size exclusion chromatography and dynamic light scattering is discussed.

Introduction

Weak protein–ligand interactions are essential in various cellular processes such as signaling cascades and metabolic pathways. The equilibrium state of a protein–ligand system depends mainly on the component concentrations and the equilibrium dissociation constant(s) of the process(es). A perturbation in the physiological environment such as change in pH or in the effector ligand concentration can shift the equilibrium of the association state. Solution small-angle X-ray scattering (SAXS) [1] is a technique that is well suited for the study of weakly interacting systems because it allows easy monitoring of association states and their structural characterization upon environmental perturbations. X-ray crystallography can provide atomic structures of stable protein–ligand complexes, although it is often not applicable when characterizing structures of low affinity complexes that are difficult to crystallize. The advantage of SAXS is that, even if it yields only low-resolution structural models, it can be used for analyzing protein–ligand complexes in a dynamic equilibrium. NMR

Abbreviations
13(S)-HODE, 13(S)-hydroxyoctadeca-9(Z),11(E)-dienoic acid; AUC, analytical ultracentrifugation; CfeSP, corrinoid iron-sulfur protein; DLS, dynamic light scattering; ITC, isothermal titration calorimetry; LOX, 12/15-lipoxygenase; MeTr, methyltransferase; PCA, principal component analysis; PKR, RNA-activated protein kinase; SA, simulated annealing; SAXS, small-angle X-ray scattering; SEC, size-exclusion chromatography; SVD, singular value decomposition; VA_1, virus-associated RNA.

spectroscopy, on the other hand, is limited by the size of complexes that can be studied, whereas SAXS measurements can be performed on systems varying from several kilodaltons to gigadaltons in size. In addition, SAXS allows the simultaneous structural and thermodynamic characterization of a complex system.

In a standard scattering experiment, protein solution is exposed to a collimated, monochromatic beam of X-rays and the angular dependence of the scattered radiation is detected (Fig. 1). The scattered radiation after subtraction of the background solvent scattering results from the mean over all orientations of the solute particles (e.g. proteins). In dilute solutions, the distribution of particles is random, and the scattering profile is continuous and radially symmetric (isotropic). As a result, the rotationally averaged scattering intensity of a particle, the scattering profile, is obtained as a function of the scattering vector $s = 4\pi\sin\theta/\lambda$, where 2θ is the scattering angle and λ is the radiation wavelength. Generally, highly purified (gel-filtration quality) samples are required for SAXS analysis, and the amount of the sample purified material is of order of hundreds of micrograms to a few milligrams, depending on the SAXS instrument and on the problem being addressed. Most advanced studies are performed on synchrotrons providing highly intense and brilliant X-ray beams, where the exposure times are in the range of tens of milliseconds, although feasible experiments can also be performed on laboratory sources, with exposures taking minutes or hours. Importantly, the purified samples do not require special preparation or labeling, and physical or chemical modifications of the sample (additions of chemical compounds, ligands, variation of temperature, pH or other parameters) are straightforward.

In a SAXS experiment, a series of samples is measured with the sample volume of approximately 10–30 μL at the solute concentrations ranging from approximately 0.1 to > 10 mg·mL^{-1}. The lower concentration limit is defined by the need to have a sufficient signal/noise ratio, whereas the upper limit depends mainly on the solubility and amount of available material. This spans a micromolar to millimolar concentration range for typical macromolecular complexes, being the most interesting range for probing weak interactions (having dissociation constants $K_d > 10^{-5}$ M). In studies of protein–ligand interactions, samples with varying protein and/or ligand concentrations are measured to monitor possible concentration-dependent changes in the scattering intensity. These changes are analyzed in terms of model-free overall parameters and the shapes of the dissolved particles, as well as in terms of the volume fractions of the components for equilibrium mixtures. Below, the major approaches employed for the analysis of SAXS data from macromolecular solutions are considered and illustrated by examples of weak protein–ligand interactions.

Model-free parameters

Immediately after SAXS data acquisition, several model-free parameters, such as the radius of gyration, R_g, the molecular mass of the particle, MM, and excluded volume, Vp, can be obtained. We discuss these parameters in the context of weakly interacting protein–ligand systems. More detailed information is also provided elsewhere [1–3].

Radius of gyration, R_g

The best known parameter determined directly from the SAXS data is the R_g [4]. When the natural logarithm of the intensity ln[$I(s)$] is plotted against the

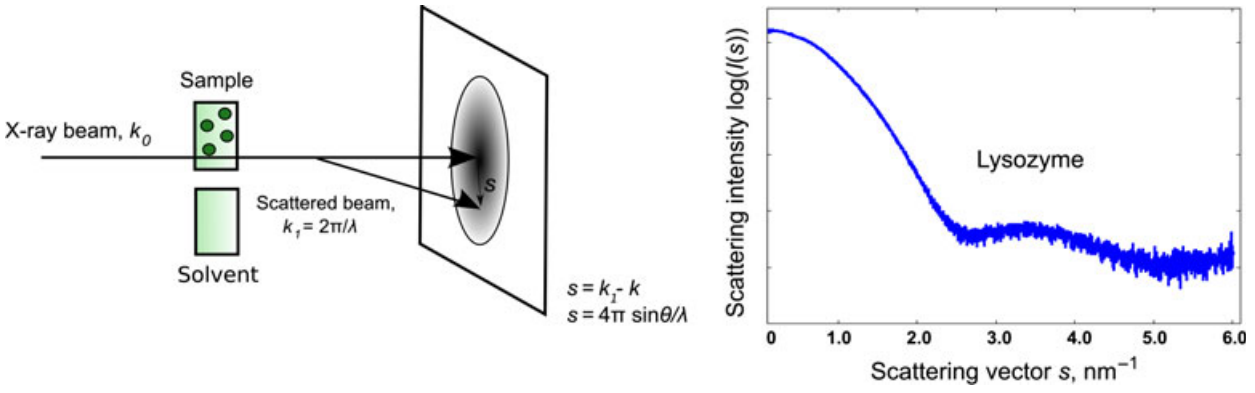

Fig. 1. SAXS experiment. The sample solution is exposed to a collimated, monochromatic beam of X-rays and the angular dependence of the scattered radiation is detected. The rotationally averaged scattering intensity of a particle as a function of the scattering vector, $s = 4\pi\sin\theta/\lambda$, where 2θ is the scattering angle and λ is the radiation wavelength, is observed.

square of the scattering vector, s^2, the y-axis intercept of the curve corresponds to the $I(0)$ value, the forward scattering at zero angle, and the slope of the linear region at low angular range ($s < 1.3\ R_g$) is directly proportional to the R_g value of a particle according to the Guinier approximation:

$$I(s) = I(0)e^{-\frac{1}{3}R_g^2 s^2} \quad (1)$$

where $I(0)$ is the scattering intensity at zero angle (Fig. 2). Typically, a series of samples with a range of concentrations of the binding partners are measured. Changes in the R_g and $I(0)$ values as a response to modifications in component concentrations reflect changes in the binding state of the system. In the case of mixtures of weakly interacting proteins, ligands and their complexes, Guinier approximation provides a mean R_g value that reflects the mean size of particles. The values of R_g can be determined with rather high accuracy (up to a few percent, i.e. for many proteins, below 1 Å), such that changes in R_g serve as a sensitive indicator of the shape and oligomeric equilibrium.

Electron pair distance distribution function, *p*(*r*), and the maximum distance of a particle, D_{max}

The scattering profile can be converted into an electron pair distance distribution function $p(r)$, a spherically averaged autocorrelation function of excess scattering density, using a so-called indirect Fourier transformation [5,6]. The $p(r)$ function is essentially a histogram of all pairwise distances, r, between electrons in the sample. Because of the rotational averaging, no directional information is available about these distances. The maximum distance in the particle D_{max} can be obtained directly from the $p(r)$ function, and an increase in the concentration of components of a weakly interacting system and complex formation is often reflected by an increase of D_{max}. A plateau in the concentration dependence of D_{max} values is reached at a concentration where the highest-order complexes starts to form or until a new higher-order complex species is included in the equilibrium. Binding of a small ligand would not yield detectable effects on the D_{max}, although ligand-binding induced structural changes in the mass distribution of the protein will alter the scattering curve and, thus, shape of the $p(r)$ function.

MM determination

SAXS data can be used to determine the MM and, hence, the oligomeric state of a protein complex. The forward scattering $I(0)$ is proportional to the square of the number of excess electrons in the particle (i.e. those exceeding the number of electrons in the solvent, excluded by the particle). Hence, the value of $I(0)$ divided by the solute concentration is proportional to the particle MM [7]. For a monodisperse system, for

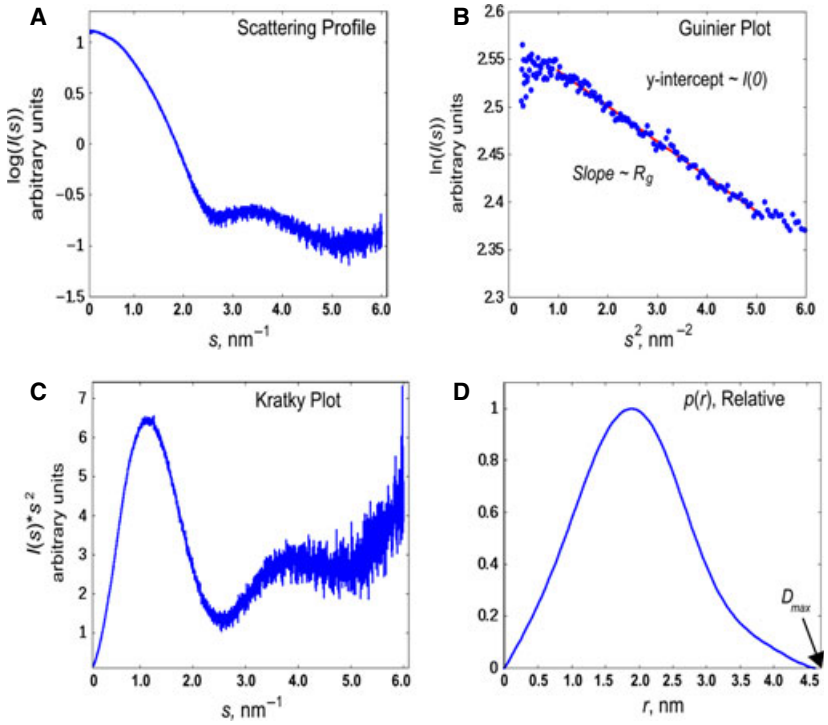

Fig. 2. Model-free parameters determined from SAXS. A scattering profile of lysozyme (A) and the corresponding Guinier plot (B). When the natural logarithm of the scattering intensity ln[$I(s)$] is plotted against square of the scattering vector s^2, the $I(0)$ value corresponds to the y-axis intercept of the curve and the R_g value the slope of the linear region at low angular range. (C) The folding state of protein–ligand system can be observed qualitatively on the basis of the Kratky plot where $s^2I(s)$ is plotted against s. Typical for a folded globular protein is a peak at low angles and the intensity decays as s^{-4} at higher angles. (D) The $p(r)$ function is essentially a histogram of all pairwise distances r between electrons in the sample. As a result of the rotational averaging, no directional information is available about the distances.

example, a tightly bound protein–ligand complex, $I(0)$ increases linearly with the concentration. When several species are present, the increase is not linear because the relative fractions of different species depend on the total protein concentration.

The forward scattering can be calculated using either the Guinier approximation or an indirect Fourier transformation to yield an MM estimate, which is independent of the particle shape. Often, the MM is computed by comparison with the forward scattering of a known standard protein such as BSA. When the concentrations of the target protein and the known standard protein are available, the MM estimate of the target protein MM_p is obtained by the equation:

$$MM_p = I_p(0)/c_p \frac{MM_{stand}}{I_{stand}(0)/c_{stand}} \quad (2)$$

where $I(0)$ and $I_{stand}(0)$ are the forward scattering of the target and standard protein, respectively, c_p and c_{stand} are the weight concentrations in mg·mL^{-1} or g·L^{-1}, and MM_{stand} is the molecular mass of the standard protein.

Porod volume, V_p

The excluded volume of the hydrated particle in solution V_p can be obtained directly from the scattering data using the *Porod* equation:

$$V_p = 2\pi^2 \frac{I(0)}{\int s^2[I(s) - K]ds} \quad (3)$$

where $I(0)$ is the forward scattering and K is a constant to ensure the asymptotic intensity decay proportional to s^{-4} at higher angles [8]. V_p provides an alternative approach for determining the effective MM_p of the solute. For globular proteins, Porod volumes (nm^3) are approximately 1.7 times the MM (kDa) [9].

Kratky plot

The folding state of protein–ligand system can be observed qualitatively using the so-called Kratky plot where $s^2I(s)$ is plotted against s [10]. A Kratky plot of a folded globular protein typically has a peak at low angles and the intensity decays as s^{-4} at higher angles. A random coil exhibits an intensity decay proportional to s^{-1} with increasing s and no distinct peak at lower angles. A comparison of Kratky plots upon titration of a ligand allows the immediate detection of folding state changes in the system. It provides a means, for example, to observe (partial) folding of a natively disordered protein upon ligand binding. This approach has been also applied to study the effect of ligand binding on the quarternary structure of RNAs [11]

Polydispersity problem

For dilute monodisperse solutions of non-interacting identical particles (e.g. for many purified protein solutions in native buffers at concentrations of appproximately 1 mg·mL^{-1}), the overall parameters are directly related to those of the single particle. For polydisperse samples containing mixtures of different particles (e.g. a protein, ligand and their complex), the interpretation of the model-free parameters becomes more complicated. The overall parameters reflect the mean over the ensemble. The effective MM is a weighted average and the R_g is the so-called z-average and the mean of R_g values of all different molecular species weighted by their scattering intensities which, hence, is sensitive to the occurrence of larger particles. Knowledge about the type of polydispersity is required for the adequate interpretation of the SAXS data from mixtures, as discussed below.

SAXS analysis of a protein–ligand equilibrium

When studying weak interactions, the binding components are often present in the sample both as individual molecules and in complex with volume fractions depending on the dissociation constant K_d. For a weakly interacting binary system, K_d specifies the relative populations of the molecular species, the protein A and the ligand B and their complex AB, present in an equilibrium:

$$AB \Leftrightarrow A + B \quad (4)$$

and the dissociation constant is defined as:

$$K_d = \frac{[A][B]}{[AB]} \quad (5)$$

where $[A]$, $[B]$ and $[AB]$ are molar concentrations of protein, ligand and complex, respectively. In a general form, the scattering profile $I(s)$ of such a mixture can be represented as a linear combination of individual scattering intensity contributions $I_i(s)$ from the different molecular species:

$$I(s) = \sum_{k=1}^{K} \eta_k \cdot I_k(s) \quad (6)$$

where η_k is the volume fraction of species k and K is the total number of components. When a set of

experiments is conducted at different concentrations, the coexisting molecular species of a weakly interacting system are present in different amounts. If the scattering intensities of the species are known (based on atomic structural models or experimental scattering data on the individual species), the volume fractions can be determined, for example, by OLIGOMER [12]. This software uses least-squares fitting to minimize the goodness-of-the-fit:

$$\chi^2 = \frac{1}{N-1}\sum_j \left(\frac{I_{\mathrm{exp}}(s_j) - cI_{\mathrm{theor}}(s_j)}{\sigma(s_j)}\right)^2 \qquad (7)$$

where N is the number of experimental points, c is a scaling factor, $I_{\mathrm{exp}}(s)$ is the experimental scattering profile, $I_{\mathrm{theor}}(s)$ is the theoretical scattering profile based on the component scattering profiles and $\sigma(s_j)$ is the experimental error. Interpretation in terms of the volume fractions provides a means to follow association/dissociation processes upon changes in environmental conditions or over time. This approach is being successfully employed to characterize the equilibria of protein or effector/ligand at varying concentrations, ionic strength, pH or temperature [13–20].

A set of SAXS experiments with varying protein or ligand concentration can be used to obtain the dissociation constant K_d. Typically, a systematic search of K_d values is carried out to determine the optimal relative fractions of A, B and AB that minimize the goodness-of-the-fit chi-squared between the resulting theoretical scattering profile and the experimental one using Eqns (5,6). This approach enables the testing of alternative structural models for a protein–ligand complex [21–23].

If the number N of different molecular species in the systems is not known in advance, a series of measurements with varying amounts of molecular species together with singular value decomposition (SVD) or principal component analysis (PCA) can be employed [24,25]. SVD and PCA are model-free approaches and no *a priori* information about the studied system is required. Note, however, that they only assess the minimum number of possible molecular species required to describe the experimental data.

Structural modeling of protein–ligand interactions against SAXS data

Ab initio modeling

In the absence of high resolution structural models, the one-dimensional SAXS data can be utilized to generate low-resolution (typically, 30–10 Å) three-dimensional models of macromolecules and their assemblies in solution *ab initio* [26–28]. At this low resolution, small ligands (e.g. chemical compounds) can of course not be detected and, in general, the ligand must be at least 10–15% in molecular mass compared to the protein to significantly alter the scattering profile. Still, binding of even small ligands could be detected indirectly if they induce larger structural rearrangements that change the overall shape of the protein (e.g. domain opening/closure) [29,30].

There are several *ab initio* approaches available [31–36]. DAMMIN/DAMMIF, comprising the most popular *ab initio* software, represent the particle as an assembly of densely packed beads placed in a search volume (typically a sphere with the diameter equal to D_{max}) and use simulated annealing (SA) to reconstruct a model by minimizing a target function R. The target function R is composed of the goodness-of-the-fit chi-squared value between the experimental and computed scattering profiles and penalties to ensure compactness and connectivity of the bead assembly.

Shape analysis is straightforward for monodisperse or almost monodisperse systems, where one of the components dominates the scattering profile. The main challenge in the *ab initio* modeling for weakly interacting systems is the decomposition of the total scattering profile into contributions from the pure molecular species for use in the individual structure reconstructions. The minimum number of species can be obtained with SVD or PCA, although a decomposition using measured SAXS profiles of the pure species is often not possible because of difficulties with respect to their isolation from a transient protein–ligand equilibrium. However, it has been shown that *ab initio* modeling of a weak complex is possible even when only a minority of the total sample (< 20%) is in the complex state [25].

Computation of scattering from high-resolution models

The use of high resolution structures or predicted models, if available, adds extremely important information for the SAXS data analysis. These approaches require accurate computation of the theoretical scattering profiles from atomic structures. For this, the spherically averaged scattering from a single macromolecule $I(s)$ can be written as:

$$I(s) = \left\langle \left| A_{\mathrm{protein}}(s) - \rho_{\mathrm{bulk}} A_{\mathrm{excluded}}(s) + (\rho_{\mathrm{hydro}} - \rho_{\mathrm{bulk}}) A_{\mathrm{layer}}(s) \right|^2 \right\rangle_{\Omega} \qquad (8)$$

where $A_{\mathrm{protein}}(s)$ is the scattering amplitude contribution from the protein in vacuum, $A_{\mathrm{excluded}}(s)$ is the

scattering amplitude from the excluded volume and $A_{layer}(s)$ is that from the hydration shell, which may have a density different from the bulk solvent.

Several methods exist for computing theoretical SAXS profiles and fitting them to experimental data. CRYSOL [37] uses implicit hydration layer model to surround the molecule with a continuous envelope of a constant adjustable electron density. FOXS presents the hydration layer implicitly based on the fractions of solvent accessible surface of atoms [38]. Alternatively, the hydration layer can be treated explicitly by introducing explicit water molecules, as in AXES [39] or HYPRED [40,41], both using molecular dynamics simulations. Another approach is to use pre-computed solvent density maps, as in AQUASAXS [42]. For protein–ligand complexes, accurate computation of the scattering intensity is important not only for validating the available models against the experimental data, but also to adequately produce the scattering profiles required for decomposition. If high-resolution models are available, theoretical profiles can be used in the Eqn (6) to determine the volume fractions of the components.

Rigid body modeling of protein–ligand complexes

Rigid-body modeling based on SAXS-data can be employed to construct molecular complexes when the structural models of the individual components are available [43,44]. SASREF [43] is one of the comprehensive rigid-body modeling approaches enabling the building of structures of molecular assemblies against SAXS data. The components (subunits or domains) are presented as rigid bodies whose relative positions and orientations are changed by an SA-based search algorithm. SASREF generates interconnected assemblies without steric clashes that minimize the target function $E(\{X\})$:

$$E(\{X\}) = \sum \chi^2\left[I_{\text{theor}}(s), I_{\exp}(s)\right] + \sum_i \alpha_i P_i \quad (9)$$

where P_i represents restraints or constraints and α_i represents the corresponding weights. Use of additional information, such as known subunit interfaces, binding affinity data or distance constraints, in the form of additional terms of P_i in the target function improves the SA search significantly. There are several examples of rigid-body modeling of weak protein–ligand complexes using SAXS data [45–48]. For example, Polizzi *et al.* [23] have determined structural models of catalytically active human UDP-α-D-xylose synthase homotetramer [23]. Only dimeric forms of the protein were observed in the earlier X-ray crystallographic structures as a result of the low affinity of the tetramer with a K_d of 2.9 μM.

When handling the systems with weakly interacting components, polydispersity of the sample can be taken into account in the structural modeling using a recently developed extended version of SASREF, namely SASREF_MX [44]. The latter software allows modeling of protein–ligand complexes in the presence of dissociation products. The experimental scattering profile is fitted by a weighted sum of the intensity contributions (Eqn 6) from the assembled complex together with those from the individual components. An SA procedure minimizes (in addition to the positions and orientations of the components in the complex) the volume fractions of the molecular species (e.g. unbound components and the bound complex). The utility of the new approach is demonstrated [44] in a number of simulated and practical examples of weak protein–protein and protein–nucleic acid complexes.

Validation of SAXS-based models and hybrid approaches

Building three-dimensional models from SAXS data is inherently ambiguous as a result of the rotational averaging, and the analysis is typically carried out several times independently to estimate the variability of the solution and to find the most typical model. The ambiguity of model reconstruction can be evaluated [9] by hierarchical clustering on the basis of C_α atom rmsd values (in the case of rigid-body modeling) or mean normalized spatial discrepancy [49] between beads (in *ab initio* modeling). The clustering provides an estimate of the stability of solutions and reveals common features in the models. The analysis can be improved further by scoring the models in a post-processing step. For rigid body models, scoring functions similar to the docking solution ranking using charge and surface complementarity and other bioinformatic tools could be employed [50–52].

The reliability of SAXS-based structural modeling improves significantly when it is performed in combination with data obtained using other techniques such as dynamic light scattering (DLS) [53,54], CD spectroscopy [55,56] or analytical ultracentrifugation (AUC) [57–59]. For example, DLS experiments yield an estimate for the molecular size based on its hydrodynamic radius R_h, which can be compared directly with the SAXS R_g value to give further indications about the oligomeric state of the system. CD spectroscopy provides information about the secondary tructure content of samples and can be related with the Kratky plots indicating the changes in flexibility

and fold of the protein upon ligand binding. Silva *et al.* [58] studied dimmers of Ydj1 and Sis1, yeast Hsp40 proteins, and their deletion mutants using SAXS in combination with DLS, AUC and CD spectroscopy [58]. *Ab initio* and rigid-body structural models of the proteins and their complexes were determined using SAXS. The oligomeric state was monitored and the models cross-validated by using the other methods.

Separation and characterization of different molecular species by combining SAXS and size-exclusion chromatography

Monodispersity is an essential requirement for many SAXS data analysis approaches. Weakly interacting protein–ligand systems rarely fulfill this requirement. One of the possibilities of obtaining more information about the bound state is to adjust the experimental conditions (e.g. pH or ionic strength) in a way that shifts the equilibrium towards the fully associated state of a complex. Another experimental option, which has reverently become available at high brilliance synchrotron beamlines, is the use of size-exclusion chromatography (SEC) to separate different association states immediately before the measurements. SEC separates macromolecular complexes based on their size and shape (R_h). The combination of synchrotron SAXS measurements with online SEC provides a powerful tool for separating and characterizing different molecular species existing in a protein–ligand equilibrium or to follow a reaction triggered by a change in environmental conditions [60–65]. The sample eluted from a size-exclusion column is directly exposed to X-rays and the scattering intensity is measured continuously as the sample flows through a measurement capillary. It is often possible to fractionate a complex from its individual components and also from unspecific aggregates. This ensures that the SAXS measurements are carried out on monodisperse and homogeneous solutions and the successive SAXS profiles can be related to different association states of the system. Several implementations of this set-up are available at different synchrotron radiation facilities around the world, including ID-18 BioSAXS/APS (USA), BL4.2/SSRL (USA), SWING/SOLEIL (France), BM-29/ESRF (France) and SR13 ID01/Australian Synchrotron (Australia).

A limitation of the SEC approach is the possibility that weakly-bound isolated complex could form a new equilibrium with a fraction of free ligand during the SAXS measurement. Hence, monitoring of additional biophysical data and the stability of the R_g when the sample flows through the SAXS capillary works as a quality control to detect whether this type of re-equilibration takes place or not. At the beamline P12 of the EMBL (storage ring Petra-3; Hamburg, Germany), a SEC system is equipped with a multidetector array for further characterization of protein–ligand and other macromolecular systems (Malvern Instruments Inc., Malvern, UK). The set-up contains detectors for measuring refractive index, right angle light scattering and UV spectra of the samples, which are first separated by SEC. The biophysical data can then be correlated with the measured continuum of SAXS profiles yielding reliable assignment of the measured molecular species.

Examples of SAXS studies of weak protein–ligand interactions

There are numerous examples of SAXS studies of protein–ligand interactions in the literature. Below, we present some selected applications, where different approaches were employed to characterize weak interactions and transient complexes. Other excellent examples can be found in recent reviews [2,3] or original papers [20,26,29,53,56,64].

12/15-lipoxygenase and its transient ligand-dependent interactions

A recent study on 12/15-lipoxygenase (LOXs) demonstrates the feasibility of SAXS to detect weak ligand-controlled protein–protein interactions [47]. Lipozygenases are a family of proteins peroxidizing lipids. The enzyme was originally assumed to function as a monomer having a single binding site for its substrate and product [66]. However, an earlier SAXS study suggested that it exists in a monomer–dimer equilibrium controlled by the ionic strength of the solution and the protein concentration [67]. Also, the crystallographic structure of 15S-LOX inhibitor complex from rabbit presents the protein in a dimeric state (Protein Data Bank code: 2P0M) [68]. The monomers in the crystallographic structure have different conformations: one monomer with bound inhibitor in the ligand binding site and the other one without a ligand. The questions remaining were whether the dimeric form in the crystals represents a biologically active structure and, if so, what is the role of ligands with respect to promoting the weak protein–protein interaction. A mechanism was proposed based on allosteric effectors that would induce the association of 12/15-LOX monomers in solution. An effector ligand would induce protein–protein binding and, consequently, one

subunit would act as an allosteric partner modulating the activity of the other subunit. To test this hypothesis, Ivanov and coworkers measured the SAXS profiles of LOX in the presence of a 13(S)-hydroxyoctadeca-9 (Z),11(E)-dienoic acid [13(S)-HODE] ligand at various concentrations as well as in the absence of the ligand [47]. Upon the addition of a 10-fold molar excess of 13(S)-HODE, the R_g of LOX increased from 3.1 ± 0.1 nm (ligand-free) to 4.2 ± 0.1 nm (ligand-excess). The latter value is similar to the theoretical R_g of approximately 4.11 nm calculated based on the crystal dimeric structure. The volume fractions of individual species were estimated using OLIGOMER representing the scattering profile as a linear combination of profiles based on the crystal structures (monomer and dimer) or on the rigid-body models produced using SASREF (Fig. 3). The major fraction of wild-type ligand-free enzyme was found in the monomeric state (approximately 85%) and only small amount in dimeric form (approximately 15%) based on analysis using OLIGOMER (a discrepancy value of $\chi = 1.38$). The dimeric volume fraction increased to approximately 95% upon the addition of 10-fold molar excess of 13 (S)-HODE, which is consistent with the change in R_g. Hence, the presence of an allosteric ligand shifted the monomer–dimer equilibrium towards the dimeric form. To support this finding, SAXS measurements were also performed on mutant enzymes where some key residues at the dimeric interface were changed. Introduction of negatively-charged residues at the interface disturbed the interaction and changed the equilibrium state. The findings based on SAXS data were correlated with molecular dynamics simulations data indicating that the dimeric complex is stable in the presence of the substrate. This example demonstrates how allosteric effects of binding can be detected using SAXS.

SAXS study of transient B_{12}-dependent methyltransferase complexes

Another example of using SAXS to detect weak protein–ligand complexes is the study of the interaction between methyltransferase (MeTr) and corrinoid iron-sulfur protein (CFeSP), comprising part of the Wood–Ljungdahl pathways and catalyzing the transfer of a one-carbon methyl unit [69,70]. The structures of these proteins have been solved individually and in the complex using X-ray crystallography, showing that MeTr works as a homodimer each subunit binding one CH_3-H_4folate [71,72], whereas CFeSP is a heterodimer consisting of a small TIM-barrel fold subunit and a large three-domain subunit with an iron sulphur clustering [73]. Ando *et al.* [69] wanted to observe the solution structures of these proteins and to obtain stoichiometric information about the transient interaction in different chemical environments. Accordingly, they measured a series of scattering profiles in a subunit titration experiment by titrating CFeSP into 50 μM MeTr. OLIGOMER was employed to fit the data with theoretical scattering profiles based on the available experimental structures. Linear combinations of free MeTr, free CFeSP and the 1 : 1 complex of them yielded good fits to the experimental data (Fig. 4). The 1 : 1 complex was maximally formed when equimolar concentrations of MeTr and CFeSP were present in the sample. When a 2 : 1 complex was added to the OLIGOMER analysis, its obtained volume fraction was found to be negligible. An *ab initio* model reconstruction at 150 μM of CFeSP, at a concentration well above the reported K_M value of 12–60 μM, agrees well with the model of the 1 : 1 complex. The concentration dependence of R_g was observed in the presence of equimolar mixtures of CFeSP and MeTR

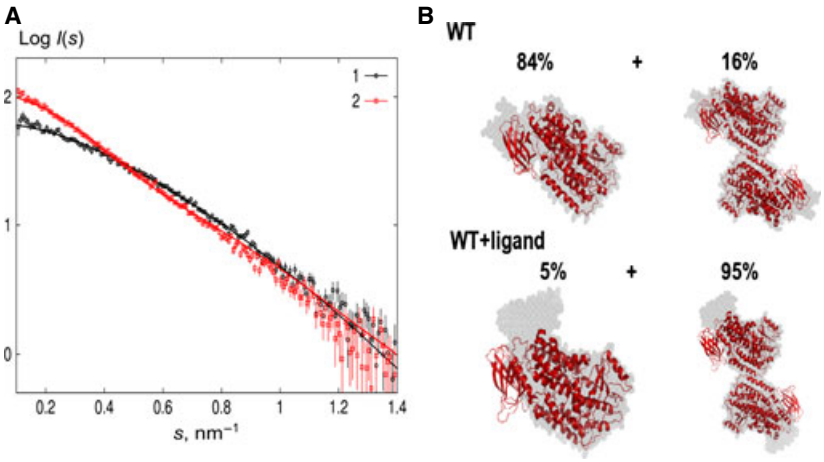

Fig. 3. SAXS profiles of 12/15-lipoxygenase with and without the ligand 13(S)-HODE. (A) The experimental SAXS profiles and fits of ligand-free (black circles and line 1) and ligand-bound (red squares and line 2) 12/15-LOX. The fits and volume fractions were obtained using OLIGOMER and the crystallographic models of the monomer and the P2-symmetry related dimer. (B) Comparison of the crystallographic structures (red ribbon; Protein Data Bank code: 2P0M) and the dimer obtained by rigid-body modeling (gray). Reproduced with permission [47].

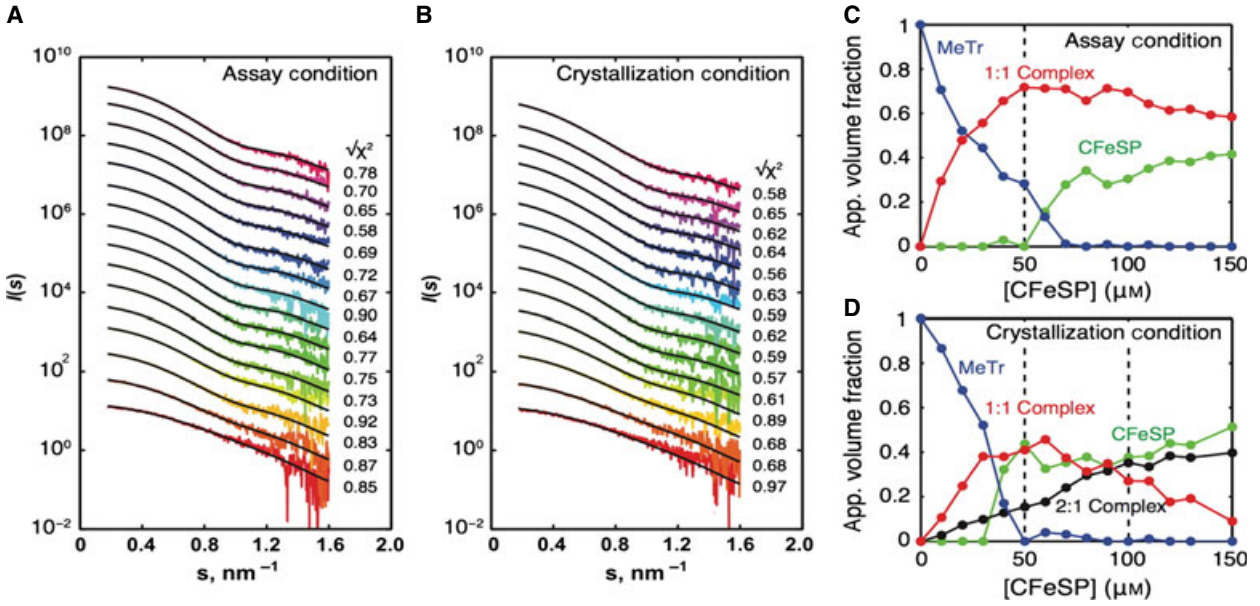

Fig. 4. SAXS analysis of MeTr–CfeSP complex stoichiometry. (A, C) The subunit stoichiometry in the MeTr–CfeSP complex was determined by measuring SAXS profiles with the titration of 0–150 μM CFeSP into MeTr homodimer (50 μM) under assay conditions. (B, D) The macromolecular crowding agent polyethylene glycol (crystallization condition) was found to promote the 2 : 1 complex formation and abolish negative co-operativity. Reproduced with permission [69].

and at different ionic strength conditions. The R_g value was found to decrease nonlinearly at concentrations < 50 μM at high ionic strength condition, indicating that salt bridge/electrostatic interactions contribute to the complex stability. The SAXS results showing that 1 : 1 complex formation is favored over the 2 : 1 complex suggests that binding of one CFeSP molecule to one of the MeTr monomers reduces the affinity of binding of the second CFeSP. Isothermal titration calorimetry (ITC) was used as a complimentary method to study this negative co-operativity. The ITC data support the finding by reporting an increased entropic cost for the second binding event. Because the crystallographic complex structure also presents a 2 : 1 stoichiometric species, SAXS measurements were repeated in the crystallization conditions. The second set of subunit titration data can be fitted well using OLIGOMER only when the 2 : 1 complex is taken into account in the linear combination of SAXS profiles. The macromolecular crowding agent polyethylene glycol was found to promote the 2 : 1 complex formation and to abolish the negative co-operativity. This suggests that crowding makes the association of MeTr and CFeSP more favorable. This example shows how SAXS can provide information about complex stoichiometry and validate crystallographic structures under more physiological solution conditions.

Weak oligomerization equilibrium of unphosphorylated STAT5a in solution

An example of K_d determination using SAXS is provided by Bernadó *et al.* [21], who studied the weak oligomerization equilibrium of unphosphorylated STAT5a in solution. Scattering data were measured at several different concentrations and analyzed together with crystallographic models of the STAT5a core domain. In the initial analysis of model-free parameters, an increase in the effective molecular weight, R_g and D_{max} values was observed, together with increase in the concentration suggesting concentration-dependent changes in the oligomerization state. PCA was used to obtain an independent estimation of the number of different molecular species in the system. Three eigenvectors were observed at each concentration, two having large amplitudes and the third having values oscillating around zero, suggesting that the experimental SAXS profiles contain only contributions from two molecular species. That finding is concurrent with earlier results from AUC studies indicating a monomer–dimer equilibrium [74]. To determine the dissociation constant of the equilibrium, an ensemble of 5000 potential dimeric structures were generated by rigid-body docking using FT-DOCK [75] and the crystallographic structure of a STAT5a monomer [74]. A search over a wide range of K_d values (0.1–212 μM)

with steps of 1% was conducted using the highest concentration data, the ensemble of dimeric models and OLIGOMER [12]. The top 50 solutions, with $\chi^2 = 8.36 \pm 0.79$, yielded a dissociation constant $K_d = 86 \pm 11$ μM, which is in a good agreement with AUC experiments on STAT1 [76]. The structures in the most populated structural cluster of the dimer ensemble (the optimal $R_g = 46$ Å) are very similar to the STAT5a crystallographic structure ($R_g = 46.2$ Å). The findings of Bernadó *et al*. [21] confirm the untypical antiparallel arrangement of the STAT5a dimer observed in the crystallographic structure but not seen for other STAT proteins.

Interaction of adenovirus virus associated RNA-I with RNA-activated protein kinase (PKR)

Dzananovic *et al*. [54,77] studied interactions between adenovirus virus-associated RNA (VA_1) and the interferon-induced, double-stranded PKR using SAXS in combination with DLS and AUC [54,77]. PKR is part of the human innate immune system and interacts with viral double-stranded RNAs to slow down viral growth and strengthen the interferon response. Before SAXS measurements, the monodispersity and purity of two RNA constructs, full-length VA_1 and $VA_1\Delta TS$ lacking the terminal stem, and a complex comprising $VA_1\Delta TS$ and the tandem N-terminal double-stranded RNA binding motifs (residues 1–169) of PKR were assured by SEC to separate unbound components and allow DLS characterization. The hydrodynamic radii R_h of VA_1 and $VA_1\Delta TS$ are 3.80 ± 0.04 nm and 3.30 ± 0.04 nm, respectively, based on DLS measurements at several concentrations. Comparable values of radii of gyration were obtained using the measured SAXS data, with an R_g of VA1 and VA1ΔTS of 4.35 ± 0.07 nm and 3.71 ± 0.06 nm, respectively. The R_h of the $VA_1\Delta TS$–$PKR_{1–169}$ complex was found to be slightly larger than that of the RNA alone (3.90 ± 0.20 nm). The stability of R_g and R_h values over a wide range of concentrations indicates monodispersity of the samples. Full-length PKR was disregarded from SAXS-based modeling approaches because the R_g, as well as the R_h, exhibited severe concentration dependence as a result of self-association. *Ab initio* structural models of VA_1, $PKR_{1–169}$ and their complex (single and two-phase models) were determined using SAXS data and cross-validated by DLS, AUC and the hydrodynamic parameters determined computationally from the models. In addition, *ab initio* SAXS structures were used as restraints to filter *in silico* generated models of $VA_1\Delta TS$ and its complex with $PKR_{1–169}$ for refinement. The combination of SAXS measurements with DLS and AUC contributes to the understanding of how VA_1 RNA binding inhibits the function and self-association of PKR and demonstrates the general applicability of this hybrid approach in the study of protein–ligand interactions.

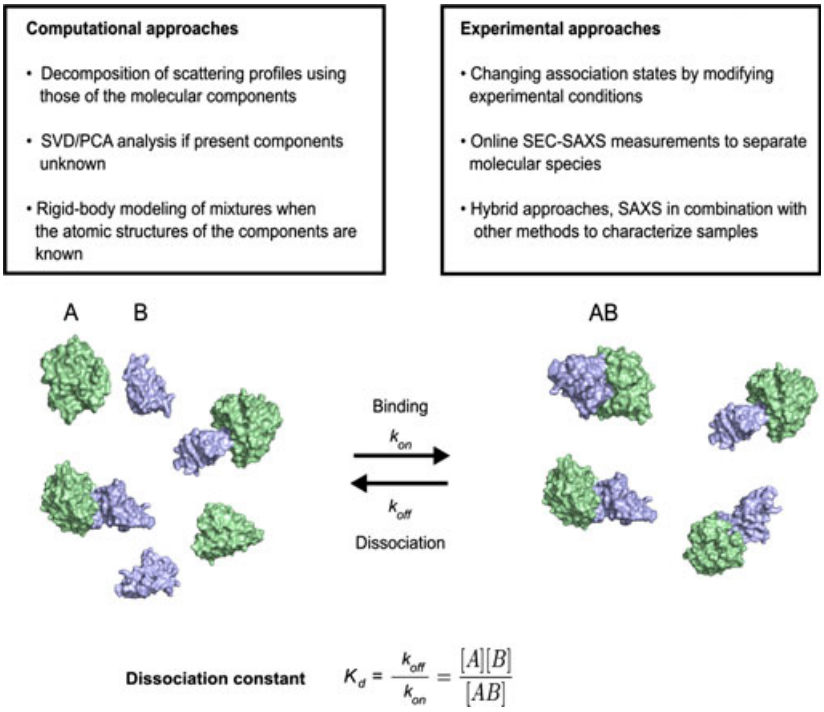

Fig. 5. Approaches for studying weak protein–ligand interactions using SAXS. The polydispersity problem of weakly interacting complexes can be handled using advanced computational methods or experimental approaches that enable more detailed characterization of the studied system and/or separation of different molecular species in the sample.

Conclusions

Interest in using SAXS to study biological systems has increased significantly during the recent years as a result of the dedicated high brilliance synchrotron beamlines and advanced data analysis methods that have become available. These developments have also made it possible to handle polydisperse and weakly interacting systems. SAXS measurements enable simultaneous structural and thermodynamic analysis of a weakly interacting molecular system in dynamic equilibrium. Two main approaches to solve the polydispersity problem can be distinguished in the study of transient protein–ligand complexes (Fig. 5). The polydispersity problem can be tackled at the sample preparation phase by using SEC to separate different association states before starting measurements or by optimizing the experimental conditions to shift the equilibrium towards a fully associated state. The second option is to deal with the polydispersity in the data analysis phase by using advanced algorithms capable of handling simultaneous scattering from several different molecular species in a mixture. New computational developments such as SASREF_MX [44] will further facilitate analysis of weakly bound protein–ligand complexes.

SAXS is a low resolution method and benefits greatly from synergistic use with other techniques, especially in the case of transient complexes whose stoichiometries are not known. In hybrid approaches, DLS data (or those from binding assays) are combined with SAXS measurements, allowing for a better sample characterization before the SAXS experiment and for an accurate assignment of association states. In the future, SAXS may become a routine tool in studies of weak protein–ligand interactions. Importantly, X-ray experiments can be performed on modern synchrotrons in millisecond time frames, allowing an analysis of kinetic processes in time-resolved SAXS studies [78–80].

Acknowledgements

A.T.T. was supported by the EMBL Interdisciplinary Postdoc Programme (EIPOD) under Marie Curie COFUND actions.

References

1 Svergun DI, Koch MHJ, Timmins PA & May RP (2013) Small Angle X-Ray and Neutron Scattering from Solutions of Biological Macromolecules. Oxford University Press, Oxford, UK.
2 Rambo RP & Tainer JA (2013) Super-resolution in solution X-ray scattering and its applications to structural systems biology. *Annu Rev Biophys* **42**, 415–441.
3 Pérez J & Nishino Y (2012) Advances in x-ray scattering: from solution SAXS to achievements with coherent beams. *Curr Opin Struct Biol* **22**, 670–678.
4 Guinier A (1939) La diffraction des rayons X aux tres petits angles: application a l'étude de phénomenes ultramicroscopiques. *Ann Phys* **12**, 161–237.
5 Glatter O (1977) A new method for the evaluation of small-angle scattering data. *J Appl Crystallogr* **10**, 415–421.
6 Svergun DI (1992) Determination of the regularization parameter in indirect-transform methods using perceptual criteria. *J Appl Crystallogr* **25**, 495–503.
7 Mylonas E & Svergun DI (2007) Accuracy of molecular mass determination of proteins in solution by small-angle X-ray scattering. *J Appl Crystallogr* **40**, 245–249.
8 Porod G (1982) General theory. In Small-angle X-ray Scattering (Glatter O & Kratky O, eds), pp. 17–52. Academic Press, London, UK.
9 Petoukhov MV, Franke D, Shkumatov AV, Tria G, Kikhney AG, Gajda M, Gorba C, Mertens HDT, Konarev PV & Svergun DI (2012) New developments in the ATSAS program package for small-angle scattering data analysis. *J Appl Crystallogr* **45**, 342–350.
10 Kratky O & Porod G (1949) Röntgenuntersuchung gelöster Fadenmoleküle. *Recl Trav Chim Pays-Bas* **68**, 1106–1122.
11 Baird NJ & Ferré-D'Amaré AR (2014) Analysis of riboswitch structure and ligand binding using small-angle x-ray scattering (SAXS). *Methods Mol Biol* **1103**, 211–225.
12 Konarev PV, Volkov VV, Sokolova AV, Koch MHJ & Svergun DI (2003) PRIMUS: a Windows PC-based system for small-angle scattering data analysis. *J Appl Crystallogr* **36**, 1277–1282.
13 Goettig P, Brandstetter H, Groll M, Göhring W, Konarev PV, Svergun DI, Huber R & Kim J-S (2005) X-ray snapshots of peptide processing in mutants of tricorn-interacting factor F1 from *Thermoplasma acidophilum*. *J Biol Chem* **280**, 33387–33396.
14 Xu X, Reinle W, Hannemann F, Konarev PV, Svergun DI, Bernhardt R & Ubbink M (2008) Dynamics in a pure encounter complex of two proteins studied by solution scattering and paramagnetic NMR spectroscopy. *J Am Chem Soc* **130**, 6395–6403.
15 Shiozawa K, Konarev PV, Neufeld C, Wilmanns M & Svergun DI (2009) Solution structure of human Pex5-Pex14-PTS1 protein complexes obtained by small angle X-ray scattering. *J Biol Chem* **284**, 25334–25342.
16 Paravisi S, Fumagalli G, Riva M, Morandi P, Morosi R, Konarev PV, Petoukhov MV, Bernier S, Chênevert

R, Svergun DI *et al*. (2009) Kinetic and mechanistic characterization of *Mycobacterium tuberculosis* glutamyl-tRNA synthetase and determination of its oligomeric structure in solution. *FEBS J* **276**, 1398–1417.
17 Wang X, Watson C, Sharp JS, Handel TM & Prestegard JH (2011) Oligomeric structure of the chemokine CCL5/RANTES from NMR, MS, and SAXS data. *Structure* **19**, 1138–1148.
18 Carvalho JWP, Santiago PS, Batista T, Salmon CEG, Barbosa LRS, Itri R & Tabak M (2012) On the temperature stability of extra-cellular hemoglobin of *Glossoscolex paulistus*, at different oxidation states: SAXS and DLS studies. *Biophys Chem* **163–164**, 44–55.
19 Jensen MH, Wahlund P-O, Toft KN, Jacobsen JK, Steensgaard DB, van de Weert M, Havelund S & Vestergaard B (2013) Small angle X-ray scattering-based elucidation of the self-association mechanism of human insulin analogue Lys(B29)(N(ε)-carboxyheptadecanoyl) des(B30). *Biochemistry* **52**, 282–294.
20 Cross PJ & Parker EJ (2013) Allosteric inhibitor specificity of *Thermotoga maritima* 3-deoxy-d-arabino-heptulosonate 7-phosphate synthase. *FEBS Lett* **587**, 3063–3068.
21 Bernadó P, Pérez Y, Blobel J, Fernández-Recio J, Svergun DI & Pons M (2009) Structural characterization of unphosphorylated STAT5a oligomerization equilibrium in solution by small-angle X-ray scattering. *Protein Sci* **18**, 716–726.
22 Kutter S, Weiss MS, Wille G, Golbik R, Spinka M & König S (2009) Covalently bound substrate at the regulatory site of yeast pyruvate decarboxylases triggers allosteric enzyme activation. *J Biol Chem* **284**, 12136–12144.
23 Polizzi SJ, Walsh RM Jr, Le Magueres P, Criswell AR & Wood ZA (2013) Human UDP–α-D-xylose synthase forms a catalytically important tetramer that has not been observed in crystal structures. *Biochemistry* **52**, 3888–3898.
24 Williamson TE, Craig BA, Kondrashkina E, Bailey-Kellogg C & Friedman AM (2008) Analysis of self-associating proteins by singular value decomposition of solution scattering data. *Biophys J* **94**, 4906–4923.
25 Blobel J, Bernadó P, Svergun DI, Tauler R & Pons M (2009) Low-resolution structures of transient protein–protein complexes using small-angle X-ray scattering. *J Am Chem Soc* **131**, 4378–4386.
26 Mallam AL, Jarmoskaite I, Tijerina P, Del Campo M, Seifert S, Guo L, Russell R & Lambowitz AM (2011) Solution structures of DEAD-box RNA chaperones reveal conformational changes and nucleic acid tethering by a basic tail. *Proc Natl Acad Sci USA* **108**, 12254–12259.
27 Bunney TD, Esposito D, Mas-Droux C, Lamber E, Baxendale RW, Martins M, Cole A, Svergun D, Driscoll PC & Katan M (2012) Structural and functional integration of the PLCγ interaction domains critical for regulatory mechanisms and signaling deregulation. *Structure* **20**, 2062–2075.
28 Zhao W, Saro D, Hammel M, Kwon Y, Xu Y, Rambo RP, Williams GJ, Chi P, Lu L, Pezza J *et al*. (2014) Mechanistic insights into the role of Hop2-Mnd1 in meiotic homologous DNA pairing. *Nucleic Acids Res* **42**, 906–917.
29 Ashish, Juncadella IJ, Garg R, Boone CD, Anguita J & Krueger JK (2008) Conformational rearrangement within the soluble domains of the CD4 receptor is ligand-specific. *J Biol Chem* **283**, 2761–2772.
30 Vohlander Rasmussen LC, Oliveira CL, Pedersen JS, Sperling-Petersen HU & Mortensen KK (2011) Structural transitions of translation initiation factor IF2 upon GDPNP and GDP binding in solution. *Biochemistry* **50**, 9779–9787.
31 Svergun DI (1999) Restoring low resolution structure of biological macromolecules from solution scattering using simulated annealing. *Biophys J* **76**, 2879–2886.
32 Chacón P, Díaz JF, Morán F & Andreu JM (2000) Reconstruction of a protein form with X-ray solution scattering and a genetic algorithm. *J Mol Biol* **299**, 1289–1302.
33 Walther D, Cohen FE & Doniach S (2000) Reconstruction of low-resolution three-dimensional density maps from one-dimensional small-angle X-ray solution scattering data for biomolecules. *J Appl Crystallogr* **33**, 350–363.
34 Svergun DI, Petoukhov MV & Koch MHJ (2001) Determination of domain structure of proteins from X-ray solution scattering. *Biophys J* **80**, 2946–2953.
35 Heller WT, Abusamhadneh E, Finley N, Rosevear PR & Trewhella J (2002) The solution structure of a cardiac troponin C-troponin I-troponin T complex shows a somewhat compact troponin C interacting with an extended troponin I-troponin T component. *Biochemistry* **41**, 15654–15663.
36 Franke D & Svergun DI (2009) DAMMIF, a program for rapid *ab-initio* shape determination in small-angle scattering. *J Appl Crystallogr* **42**, 342–346.
37 Svergun D, Barberato C & Koch MHJ (1995) CRYSOL – a program to evaluate X-ray solution scattering of biological macromolecules from atomic coordinates. *J Appl Crystallogr* **28**, 768–773.
38 Schneidman-Duhovny D, Hammel M & Sali A (2010) FoXS: a web server for rapid computation and fitting of SAXS profiles. *Nucleic Acids Res* **38** (Web Server issue), W540–W544.
39 Grishaev A, Guo L, Irving T & Bax A (2010) Improved fitting of solution X-ray scattering data to

macromolecular structures and structural ensembles by explicit water modelling. *J Am Chem Soc* **132**, 15484–15486.
40 Virtanen JJ, Makowski L, Sosnick TR & Freed KF (2010) Modeling the hydration layer around proteins: HyPred. *Biophys J* **99**, 1611–1619.
41 Virtanen JJ, Makowski L, Sosnick TR & Freed KF (2011) Modeling the hydration layer around proteins: applications to small- and wide-angle X-ray scattering. *Biophys J* **101**, 2061–2069.
42 Poitevin F, Orland H, Doniach S, Koehl P & Delarue M (2011) AquaSAXS: a web server for computation and fitting of SAXS profiles with non-uniformally hydrated atomic models. *Nucleic Acids Res* **39** (Web Server issue), W184–W189.
43 Petoukhov MV & Svergun DI (2005) Global rigid body modeling of macromolecular complexes against small-angle scattering data. *Biophys J* **89**, 1237–1250.
44 Petoukhov MV & Svergun DI (2013) Applications of small-angle X-ray scattering to biomacromolecular solutions. *Int J Biochem Cell Biol* **45**, 429–437.
45 Singh RK, Larson JD, Zhu W, Rambo RP, Hura GL, Becker DF & Tanner JJ (2011) Small-angle X-ray scattering studies of the oligomeric state and quaternary structure of the trifunctional proline utilization A (PutA) flavoprotein from *Escherichia coli*. *J Biol Chem* **286**, 43144–43153.
46 Street TO, Lavery LA & Agard DA (2011) Substrate binding drives large-scale conformational changes in the Hsp90 molecular chaperone. *Mol Cell* **42**, 96–105.
47 Ivanov I, Shang W, Toledo L, Masgrau L, Svergun DI, Stehling S, Gómez H, Di Venere A, Mei G, Lluch JM *et al*. (2012) Ligand-induced formation of transient dimers of mammalian 12/15-lipoxygenase: a key to allosteric behavior of this class of enzymes? *Proteins* **80**, 703–712.
48 Ohbayashi N, Matsumoto T, Shima H, Goto M, Watanabe K, Yamano A, Katoh Y, Igarashi K, Yamagata Y & Murayama K (2013) Solution structure of clostridial collagenase H and its calcium-dependent global conformation change. *Biophys J* **104**, 1538–1545.
49 Kozin MB & Svergun DI (2001) Automated matching of high- and low-resolution structural model. *J Appl Crystallogr* **34**, 33–41.
50 Andreani J, Faure G & Guerois R (2013) InterEvScore: a novel coarse-grained interface scoring function using a multi-body statistical potential coupled to evolution. *Bioinformatics* **29**, 1742–1749.
51 Khashan R, Zheng W & Tropsha A (2012) Scoring protein interaction decoys using exposed residues (SPIDER): a novel multibody interaction scoring function based on frequent geometric patterns of interfacial residues. *Proteins* **80**, 2207–2217.
52 Hwang H, Vreven T, Pierce BG, Hung J-H & Weng Z (2010) Performance of ZDOCK and ZRANK in CAPRI rounds 13-19. *Proteins* **78**, 3104–3110.
53 Calcutta A, Jessen CM, Behrens MA, Oliveira CL, Renart ML, González-Ros JM, Otzen DE, Pedersen JS, Malmendal A & Nielsen NC (2012) Mapping of unfolding states of integral helical membrane proteins by GPS-NMR and scattering techniques: TFE-induced unfolding of KcsA in DDM surfactant. *Biochim Biophys Acta* **1818**, 2290–2301.
54 Dzananovic E, Patel TR, Chojnowski G, Boniecki MJ, Deo S, McEleney K, Harding SE, Bujnicki JM & McKenna SA (2014) Solution conformation of adenovirus virus associated RNA-I and its interaction with PKR. *J Struct Biol* **185**, 48–57.
55 Zagrovic B, Lipfert J, Sorin EJ, Millett IS, van Gunsteren WF, Doniach S & Pande VS (2005) Unusual compactness of a polyproline type II structure. *Proc Natl Acad Sci USA* **102**, 11698–11703.
56 Mallik L, Arif E, Sharma P, Rathore YS, Wong HN, Holzman LB, Ashish & Nihalani D (2012) Solution structure analysis of cytoplasmic domain of podocyte protein Neph1 using small/wide angle X-ray scattering (SWAXS). *J Biol Chem* **287**, 9441–9453.
57 Yang C, van der Woerd MJ, Muthurajan UM, Hansen JC & Luger K (2011) Biophysical analysis and small-angle X-ray scattering-derived structures of MeCP2-nucleosome complexes. *Nucleic Acids Res* **39**, 4122–4135.
58 Silva JC, Borges JC, Cyr DM, Ramos CH & Torriani IL (2011) Central domain deletions affect the SAXS solution structure and function of yeast Hsp40 proteins Sis1 and Ydj1. *BMC Struct Biol* **11**, 40–53.
59 Gabrielsen M, Beckham KS, Feher VA, Zetterström CE, Wang D, Müller S, Elofsson M, Amaro RE, Byron O & Roe AJ (2012) Structural characterisation of Tpx from *Yersinia pseudotuberculosis* reveals insights into the binding of salicylidene acylhydrazide compounds. *PLoS One* **7**, e32217.
60 Mathew E, Mirza A & Menhart N (2004) Liquid-chromatography-coupled SAXS for accurate sizing of aggregating proteins. *J Synchrotron Radiat* **11**, 314–318.
61 David G & Pérez J (2009) Combined sampler robot and high-performance liquid chromatography: a fully automated system for biological small-angle X-ray scattering experiments at the Synchrotron SOLEIL SWING beamline. *J Appl Crystallogr* **42**, 892–900.
62 Jensen MH, Toft KN, David G, Havelund S, Pérez J & Vestergaard B (2010) Time-resolved SAXS measurements facilitated by online HPLC buffer exchange. *J Synchrotron Radiat* **17**, 769–773.
63 Rambo RP & Tainer JA (2010) Improving small-angle X-ray scattering data for structural analyses of the RNA world. *RNA* **16**, 638–646.

64 Didry D, Cantrelle F-X, Husson C, Roblin P, Moorthy AM, Pérez J, Le Clainche C, Hertzog M, Guittet E, Carlier M-F *et al*. (2012) How a single residue in individual β-thymosin/WH2 domains controls their functions in actin assembly. *EMBO J* **31**, 1000–1013.
65 Round A, Brown E, Marcellin R, Kapp U, Westfall CS, Jez JM & Zubieta C (2013) Determination of the GH3.12 protein conformation through HPLC-integrated SAXS measurements combined with X-ray crystallography. *Acta Crystallogr D Biol Crystallogr* **69**, 2072–2080.
66 de Luca C & Olefsky JM (2008) Inflammation and insulin resistance. *FEBS Lett* **582**, 97–105.
67 Shang W, Ivanov I, Svergun DI, Borbulevych OY, Aleem AM, Stehling S, Jankun J, Kühn H & Skrzypczak-Jankun E (2011) Probing dimerization and structural flexibility of mammalian lipoxygenases by small-angle X-ray scattering. *J Mol Biol* **409**, 654–668.
68 Choi J, Chon JK, Kim S & Shin W (2008) Conformational flexibility in mammalian 15S-lipoxygenase: reinterpretation of the crystallographic data. *Proteins* **70**, 1023–1032.
69 Ando N, Kung Y, Can M, Bender G, Ragsdale SW & Drennan CL (2012) Transient B12-dependent methyltransferase complexes revealed by small-angle X-ray scattering. *J Am Chem Soc* **134**, 17945–17954.
70 Ragsdale SW (2008) Enzymology of the Wood-Ljungdahl pathway of acetogenesis. *Ann N Y Acad Sci* **1125**, 129–136.
71 Doukov TI, Seravalli J, Stezowski JJ & Ragsdale SW (2000) Crystal structure of a methyltetrahydrofolate- and corrinoid-dependent methyltransferase. *Structure* **8**, 817–830.
72 Doukov TI, Hemmi H, Drennan CL & Ragsdale SW (2007) Structural and kinetic evidence for an extended hydrogen-bonding network in catalysis of methyl group transfer. Role of an active site asparagine residue in activation of methyl transfer by methyltransferases. *J Biol Chem* **282**, 6609–6618.
73 Kung Y, Ando N, Doukov TI, Blasiak LC, Bender G, Seravalli J, Ragsdale SW & Drennan CL (2012) Visualizing molecular juggling within a B12-dependent methyltransferase complex. *Nature* **484**, 265–269.
74 Neculai D, Neculai AM, Verrier S, Straub K, Klumpp K, Pfitzner E & Becker S (2005) Structure of the unphosphorylated STAT5a dimer. *J Biol Chem* **280**, 40782–40787.
75 Gabb HA, Jackson RM & Sternberg MJ (1997) Modelling protein docking using shape complementarity, electrostatics and biochemical information. *J Mol Biol* **272**, 106–120.
76 Mao X, Ren Z, Parker GN, Sondermann H, Pastorello MA, Wang W, McMurray JS, Demeler B, Darnell JE Jr & Chen X (2005) Structural bases of unphosphorylated STAT1 association and receptor binding. *Mol Cell* **17**, 761–771.
77 Dzananovic E, Patel TR, Deo S, McEleney K, Stetefeld J & McKenna SA (2013) Recognition of viral RNA stem-loops by the tandem double-stranded RNA binding domains of PKR. *RNA* **19**, 333–344.
78 Cho HS, Dashdorj N, Schotte F, Graber T, Henning R & Anfinrud P (2010) Protein structural dynamics in solution unveiled via 100-ps time-resolved X-ray scattering. *Proc Natl Acad Sci USA* **107**, 7281–7286.
79 Pollack L (2011) Time resolved SAXS and RNA folding. *Biopolymers* **95**, 543–549.
80 Kler S, Asor R, Li C, Ginsburg A, Harries D, Oppenheim A, Zlotnick A & Raviv U (2012) RNA encapsidation by SV40-derived nanoparticles follows a rapid two-state mechanism. *J Am Chem Soc* **134**, 8823–8830.